Growth and Characterization of Ternary AlGaN Alloy Nanocones across the Entire Composition Range

Chengyu He,[†] Qiang Wu,[†,*] Xizhang Wang,[†] Yongliang Zhang,[†] Lijun Yang,[†] Ning Liu,[†] Yu Zhao,[†] Yinong Lu,[‡] and Zheng Hu[†,*]

[†]Key Laboratory of Mesoscopic Chemistry of MOE, School of Chemistry and Chemical Engineering, Nanjing University, Nanjing 210093, People's Republic of China and [‡]College of Materials Science and Engineering, Nanjing University of Technology, Nanjing 210009, People's Republic of China

ABSTRACT AlGaN ternary alloys have unique properties suitable for numerous applications due to their tunable direct band gap from 3.4 to 6.2 eV by changing the composition. Herein we report a convenient chemical vapor deposition growth of the quasi-aligned $Al_xGa_{1-x}N$ alloy nanocones over the entire composition range. The nanocones were grown on Si substrates in large area by the reactions between $GaCl_3$, $AlCl_3$ vapors, and NH_3 gas under moderate temperature around 700 °C. The as-prepared wurtzite $Al_xGa_{1-x}N$ nanocones have single-crystalline structure preferentially growing along the *c*-axis, with homogeneous composition distribution, as revealed by the characterizations of electron microscopy, X-ray diffraction, energy-dispersive X-ray spectroscopy, and selected area electron diffraction. The continuous composition tunability is also demonstrated by the progressive evolutions of the band edge emission in cathodoluminescence and the turn-on and threshold fields in field emission measurements. The successful preparation of $Al_xGa_{1-x}N$ nanocones provides the new possibility for the further development of advanced nano- and opto-electronic devices.

KEYWORDS: ternary AlGaN alloy · one-dimensional nanostructures · single phase · composition regulation · chemical vapor deposition

The family of group III nitrides including AlN, GaN, InN, and their alloys have been recognized as the most important wide band gap semiconductor materials due to their successful applications in (opto)electronic devices in the past few years.[1−6] Their superior properties are demonstrated in the light emission covering continuously from the near-infrared to the ultraviolet region, excellent thermal conductivity and hardness, high resistance to chemicals, and high melting point. With the development of nanotechnology, their one-dimensional (1D) nanostructures, especially the aligned arrays, have attracted increasing interests for the potential applications in nanodevices such as nanoscale light-emitting diodes,[7] field effect transistors,[8] and nanogenerators,[9] as well as for understanding fundamental concepts underlying the observed electronic, optical, and mechanical properties of materials.[7−11] To date, various 1D nanostructures such as nanotubes, nanowires, and nanocones have been synthesized for the binary AlN,[12−14] GaN,[15−17] and InN.[18] Very recently, ternary $In_xGa_{1-x}N$ nanowires across the entire composition range were obtained, which could adjust the band gap in the range of 1.1−3.4 eV, showing the tunable emission from the near-UV to the near-infrared region.[19] For the important ternary AlGaN system with the tunable band gap at 3.4−6.2 eV,[3] however, the growth of the 1D nanostructures and composition regulation remains a challenging topic, though great efforts have been devoted to it.[11,20−27] Scientists tried to fabricate AlGaN nanowires with different methods including chemical vapor deposition (CVD), metal−organic chemical vapor deposition (MOCVD), and even molecular beam epitaxy (MBE). In the attempt to prepare homogeneously alloyed AlGaN nanowires using a CVD process, Choi *et al.* discovered a spontaneous phase separation within the AlGaN alloy nanowire system and hence obtained the GaN/AlGaN core−sheath heterostructured nanowires eventually.[21] Similarly, spontaneous formation of GaN/AlGaN coaxial nanowires is also observed by Su *et al.* in their preparation with MOCVD due to the phase separation.[22] AlGaN alloy nanowires were also attempted by CVD and plasma-assisted MBE method using metal Ga and Al sources,[24,25] but the phase separation still cannot be excluded since convincing experimental evidence of XRD with the characteristic singlet of (002) diffraction around 30−40° was not provided. In addition, the proposed AlGaN 1D nanostructures prepared by MBE and low-pressure MOCVD need further characterization.[20,23] In a word, the preparation, especially the composition regulation of 1D nanostructures for the ternary AlGaN system, has been

* Address correspondence to wqchem@nju.edu.cn, zhenghu@nju.edu.cn.

Received for review November 4, 2010 and accepted January 20, 2011.

Published online February 01, 2011
10.1021/nn1029845

© 2011 American Chemical Society

a rather tough issue to date, which may be due to the difficulty getting the matchable partial pressures of Al- and Ga-containing sources during synthesis to restrain the spontaneous tendency of the phase separation in the product.

In the past few years, we have developed a simple CVD growth of AlN nanocone arrays *via* the reaction between $AlCl_3$ vapor and NH_3 gas at moderate temperature.[13] By designing a three-temperature-zone tubular furnace which could separately adjust the partial pressures of $GaCl_3$ and $AlCl_3$ vapors for the convenient optimization of the matchable ratio, in this study, we have extended this route to the growth of ternary $Al_xGa_{1-x}N$ nanocone arrays across the entire composition range from $x = 0$ to 1. The continuous composition tunability is also demonstrated by the progressive evolution of the cathodoluminescence (CL) and field emission (FE). The successful preparation of $Al_xGa_{1-x}N$ nanocones provides the new possibility for the further development of advanced nano- and opto-electronic devices.

RESULTS AND DISCUSSION

Figure 1 shows the scanning electron microscopy (SEM), X-ray diffraction (XRD), and energy-dispersive X-ray spectroscopy (EDS) examinations on a sequence of samples (nos. 1−11) obtained by systematic regulation of the partial pressures of $GaCl_3$ and $AlCl_3$ vapors. The samples are ordered by increasing the partial pressure of $AlCl_3$, with no. 1 and no. 11 for the single $GaCl_3$ and $AlCl_3$ vapor, respectively. All of the products are composed of the quasi-aligned nanocones except for no. 1, which consists of quasi-aligned nanowires (Figure 1a) (Supporting Information, Figure S1). From Figure 1b, it is learned that the XRD patterns for no. 1 and no. 11 match well with hexagonal GaN and AlN (h-GaN, h-AlN) as expected,[13,15] which is also supported by the corresponding EDS spectrum with Ga and N or Al and N signals (Figure 1c). From no. 1 to no. 11, the three characteristic peaks of (100), (002), and (101) progressively shift toward the higher angle side (Figure 1b) accompanied by the decreasing Ga and increasing Al contents (Figure 1c) (Supporting Information, Figure S2). This indicates the successful growth of the ternary $Al_xGa_{1-x}N$ alloy nanocones across the entire composition range. The up-shifting of the characteristic peaks results from the decreasing lattice parameters *c* and *a* with increasing Al/Ga ratio due to the smaller atomic radius of Al than Ga, similar to the case for the thin-film technology.[28] The singlet of (002) diffraction without splitting for the ternary sample (no. 2−10) indicates the single-phase feature; otherwise, phase separation would be observed (Supporting Information, Figure S3).[29] The slight broadening of the (002) peak (nos. 2−10) compared to that of the binary GaN or AlN (nos. 1, 11) might arise from the intrinsic broadening for a random $Al_xGa_{1-x}N$ alloy[30] and the slight compositional fluctuation

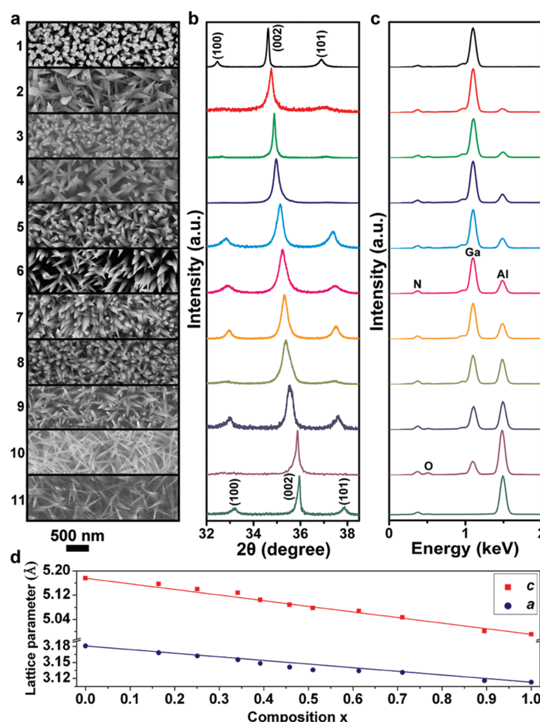

Figure 1. SEM, XRD, and EDS characterizations on a sequence of $Al_xGa_{1-x}N$ products with increasing Al content from no. 1 to no. 11. (a) SEM images. (b) XRD patterns with the characteristic peaks of (100), (002), and (101). (c) SEM-EDS spectra with marked elemental signals. (d) Lattice parameters *c* and *a* calculated from the corresponding (002) and (100) diffractions in (b) *versus* Al content determined by SEM-EDS in (c), and Vegard's law approximations for *c* and *a* as a function of Al content (red and blue lines) taking c = 5.176 and 4.991 Å and a = 3.181 and 3.113 Å for GaN and AlN, respectively. It is seen that the diffraction peaks in (b) progressively shift to the higher angle side with increasing Al content in (c). The direct correlation between the structural and compositional evolutions indicates the successful preparation of the ternary $Al_xGa_{1-x}N$ alloy nanocones across the entire composition range.

across the large area on the Si substrate. The plots of lattice parameters *c* and *a* deduced from XRD (Figure 1b) *versus* Al concentration determined by SEM-EDS (Figure 1c) show a near-linear correlation between the lattice spacing and the alloy composition, in good match with the corresponding Vegard's law approximation as seen in Figure 1d (Supporting Information, Table S1).[31] This result further supports the continuous composition regulation for $Al_xGa_{1-x}N$ alloy nanocones.

To get a deeper insight into the microstructures of the $Al_xGa_{1-x}N$ nanocones, high-resolution transmission electron microscopy (HRTEM) and corresponding selected area electron diffraction (SAED) were examined, as shown in Figure 2. HRTEM images show that each nanocone is single crystalline with the growth direction along [001], as confirmed by the corresponding SAED pattern (Supporting Information, Figure S4). Lack of large variations in contrast indicates the compositional homogeneity or no phase segregation in the nanocones, which is also supported by the respective

set of sharp diffraction spots, rather than diffused or separated ones. It is noted that the distances between the diffraction spots of (00*l*) (*l* = 1, 2, 3, 4) and the center spot slightly increase with increasing *x*, indicating the corresponding reduction of the interplanar spaces of (00*l*). Similar change is also observed for the distances between the diffraction spots of (*h*00) (*h* = 1, 2) and the center spot (Supporting Information, Figure S5). Such evolutions are in good agreement with the XRD results (Supporting Information, Table S1). The preceding results indicate that the obtained $Al_xGa_{1-x}N$ nanocones are single crystalline with tunable composition in microscale. The compositional homogeneities of the $Al_xGa_{1-x}N$ nanocones are further supported by TEM-EDS multiple-spot analysis along the individual nanocone, as shown in Figure 3, for three typical nanocones with different compositions (Supporting Information, Figure S6). The small fluctuation of the contents for Ga and Al elements along the nanocone indicates the homogeneous composition distribution over the whole nanocone for each sample. The average *x* values for the three $Al_xGa_{1-x}N$ samples are 0.20, 0.67, and 0.87 (Figure 3), in agreement with the corresponding ones obtained by SEM-EDS (Supporting Information, Table S1) within experimental errors.

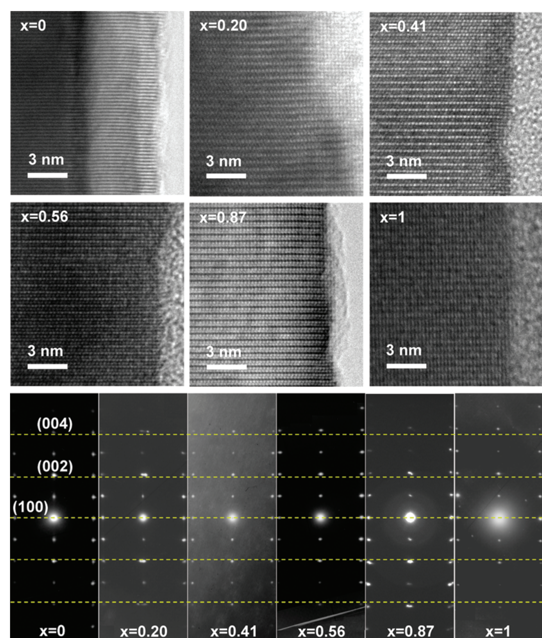

Figure 2. HRTEM images and the corresponding SAED patterns of the $Al_xGa_{1-x}N$ nanocones with increasing Al content (*x*) determined by TEM-EDS. The dashed horizontal lines are drawn over the electron diffraction images as a reference for comparison of the distances between the diffraction spots and the center spot.

The formation of the tapering morphology of the products could be understood from the different growth rates of the wurtzite crystal in different directions. As known, there is no center of inversion in the wurtzite crystal structure, and therefore, an inherent asymmetry along the *c*-axis is present which allows the anisotropic growth of the crystal along the [0001] direction.[32] The idealized growth habit should be the hexagonally prismatic crystal with two types of surfaces: the {0001} and {10−10} prism faces.[33] However, the morphology of a real crystal often deviates from the form of a perfectly hexagonal prism, and many crystals exhibit some tapering along their *c*-axes.[33] The growth rates of the crystal in different directions are the main reason to influence the crystal morphology.

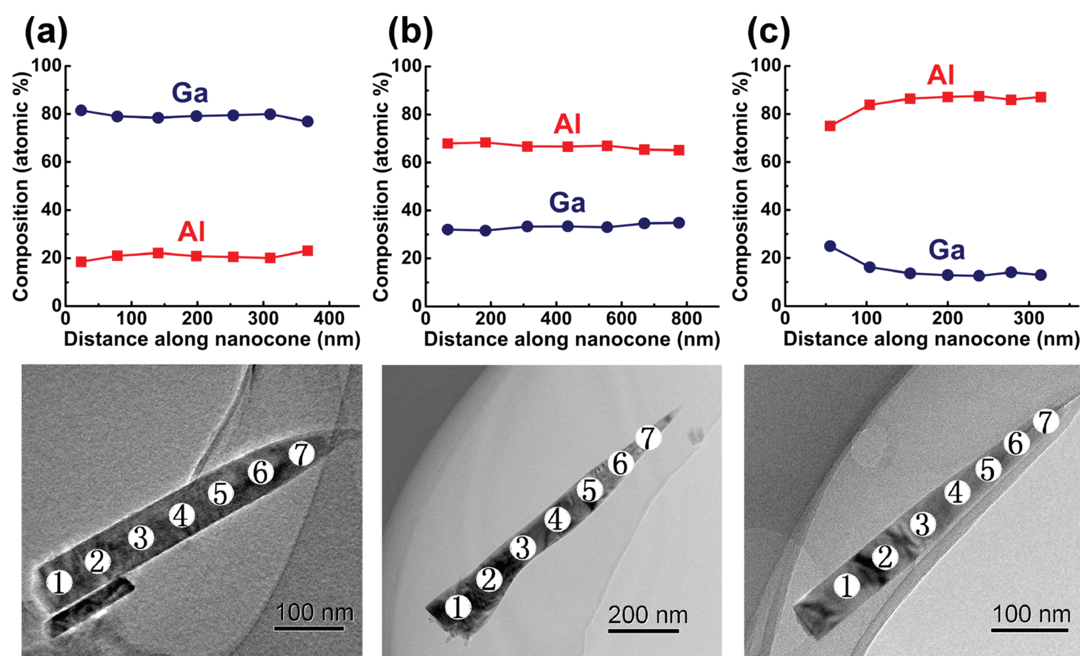

Figure 3. Multiple-spot composition analysis by using TEM-EDS for three typical nanocones with corresponding TEM images. Seven points were taken along the individual nanocone. The spot diameter of the electron beam is about 10 nm. Samples a, b, and c correspond to nos. 3, 9, and 10 in Figure 1, respectively.

Generally, the growth rate (r) in the [0001] direction is faster than those in other directions, for example, in the order of $r_{[0001]} > r_{[10-1-1]} > r_{[10-10]} > r_{[10-11]} > r_{[000-1]}$ for ZnO.[34,35] Hence, for the anisotropic growth of the wurtzite crystal, in addition to the preferential growth along c-axis, the lateral growth along ⟨10−10⟩ is unavoidable. It could be expected that the root part experiences longer time for the lateral growth and has the larger diameter, leading to the tapering along the c-axis. Thus, if the axial growth rate is too much faster than the lateral growth rate, the tapering caused by the different time of the lateral growth is negligible. In this case, the final product is more like a hexagonal prism than a cone. On the basis of the above analysis, it is speculated that, under our experimental condition, the axial growth rate is too much faster than the lateral growth rate for GaN, hence the nanowires are like the hexagonal prism formed.[36] For AlGaN or AlN, the ratio of the axial growth rate to the lateral growth rate is not as large as that for GaN, hence the tapering nanocones formed.

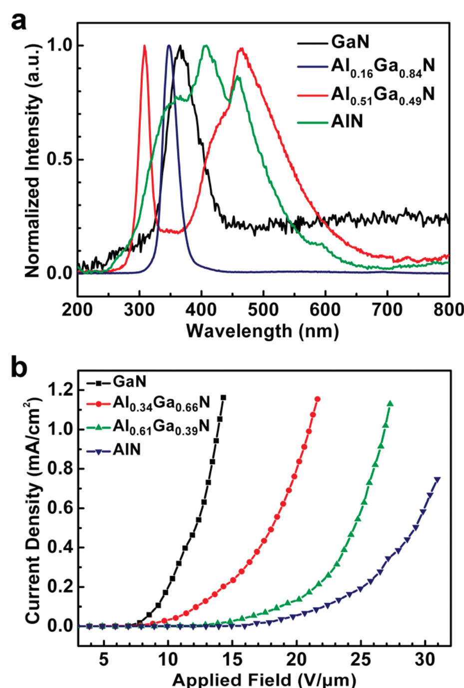

Figure 4. Progressive evolution of the optical and electrical properties for the $Al_xGa_{1-x}N$ nanocones with different compositions. (a) Normalized cathodoluminescence spectra at room temperature for GaN, $Al_{0.16}Ga_{0.84}N$, $Al_{0.51}Ga_{0.49}N$, and AlN nanocones. (b) Curves of current density *versus* the applied field ($J-E$ curves) for GaN, $Al_{0.34}Ga_{0.66}N$, $Al_{0.61}Ga_{0.39}N$, and AlN nanocones with an electrode distance of 100 μm.

On the basis of the aforementioned characterization results, it is seen that the ternary $Al_xGa_{1-x}N$ alloy nanocones across the entire composition range were successfully synthesized. The continuous composition tunability for $Al_xGa_{1-x}N$ nanocones is also demonstrated by the progressive evolution of their optical and electrical properties in the following CL and FE measurements, as shown in Figure 4.

As expected, room-temperature-normalized CL spectra of the $Al_xGa_{1-x}N$ nanocones indicate a band gap widening with increasing x, that is, Al content (Figure 4a).[37] The wavelength of the band edge emission for GaN, $Al_{0.16}Ga_{0.84}N$, and $Al_{0.51}Ga_{0.49}N$ is 366, 348, and 308 nm, corresponding to the optical band gap (E_g) of 3.40, 3.57, and 4.03 eV, respectively. It should be noted that the defect-related low-energy emission increases with Al content. For the GaN and $Al_{0.16}Ga_{0.84}N$ samples, only the band edge emissions are present, while the additional defect-related emissions appear for the Al-rich $Al_{0.51}Ga_{0.49}N$ sample, and only the defect-related emissions could be observed for the AlN sample. Incidentally, only very limited data on the optical properties are available for pure AlN due to the unavoidable oxidation and high oxygen solubility in AlN;[12,38] hence, the optical properties of AlN are much influenced by oxygen-related defects especially for AlN nanomaterials with high surface areas. FE curves of the current density *versus* the applied field ($J-E$) clearly show that the turn-on field, E_{to}, and threshold field, E_{thr} (defined as the electric fields to generate emission current densities of 10 $\mu A/cm^2$ and 1 mA/cm^2,

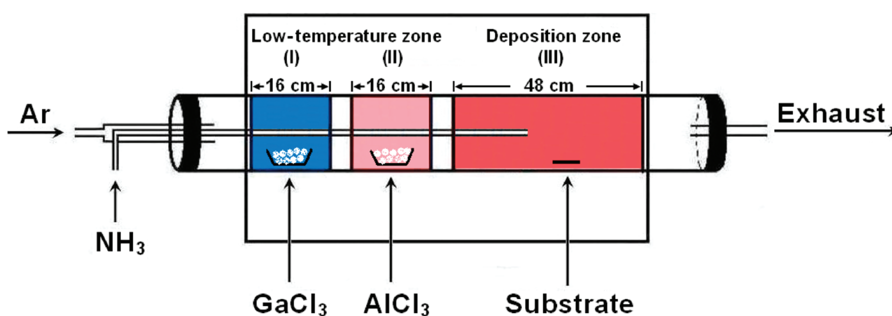

Figure 5. Experimental setup. The tubular furnace consists of three zones with independent heating apparatus. Water cooling and fan cooling are set between the connective parts to minimize the mutual interference. Anhydrous $GaCl_3$ and $AlCl_3$ powders were placed into two crucibles and put into the low-temperature zones I and II, respectively. A Si substrate (1 cm × 1 cm) was loaded in the deposition zone. The partial pressures of $GaCl_3$ and $AlCl_3$ vapors could be regulated by adjusting the corresponding evaporation temperatures. Flowing Ar was introduced at the left end as protection and carrying gas. The inlet of NH_3 is settled at the front part of the deposition zone, where NH_3 reacted with the mixture of $GaCl_3$ and $AlCl_3$ vapors to deposit AlGaN nanocone arrays on the Si substrate.

respectively), for $Al_xGa_{1-x}N$ nanocones increase with increasing Al content, that is, on the order of GaN < $Al_{0.34}Ga_{0.66}N$ < $Al_{0.61}Ga_{0.39}N$ < AlN (Figure 4b) (Supporting Information, Figure S7 and Table S2). Taking into account the fact that the work functions of the four samples are close to each other (Supporting Information, Table S3), we could infer that the reduced FE with increasing Al contents is mainly attributed to the decreasing of carrier density due to the widening of the band gap.[39] In other words, with E_g of 6.2 eV, AlN is a dielectric with poor conductivity and unfavorable for supplying electrons to the emitting tip, hence presenting the highest E_{to} and E_{thr}. Decreasing Al content in the $Al_xGa_{1-x}N$ emitters leads to the decreasing band gap, thereof the increasing conductivity, which would result in the better FE performance.[40] The progressive evolution of the CL and FE properties further demonstrates the continuous composition tunability for the obtained $Al_xGa_{1-x}N$ nanocones.

CONCLUSIONS

In summary, the quasi-aligned $Al_xGa_{1-x}N$ alloy nanocones over the entire composition range have been prepared for the first time. The nanocones were grown on Si substrates in large area by a convenient CVD growth through the reactions between $GaCl_3$, $AlCl_3$ vapors, and NH_3 gas under moderate temperature around 700 °C. The as-prepared wurtzite $Al_xGa_{1-x}N$ nanocones have single-crystalline structure preferentially growing along the *c*-axis, with homogeneous composition distribution. For 1D nanostructures of the important ternary AlGaN system, the complete composition tunability provides the possibility to tailor their properties, as demonstrated by the progressive evolutions of the band edge emission and the turn-on/threshold fields in the respective CL and FE measurements in this study, which is of great importance for the further development of advanced nano- and optoelectronic devices.

EXPERIMENTAL SECTION

The growth of AlGaN nanocones was conducted in a horizontal three-temperature-zone tubular furnace with $GaCl_3$, $AlCl_3$, and NH_3 as Ga, Al, and N sources, respectively (Figure 5). Typically, about 0.4 g of anhydrous $GaCl_3$ and $AlCl_3$ powders was separately placed at the low-temperature zones I and II and a n-type Si substrate (1 cm × 1 cm) in the high-temperature zone III (*i.e.*, the deposition zone). The system was evacuated and flushed with Ar gas several times to remove oxygen and moisture. After the deposition zone was heated to ~700 °C under the protection of Ar flow, the low-temperature zones I and II were quickly (~10 min) heated to the desired evaporation temperature of 80 °C for $GaCl_3$ and 140 °C for $AlCl_3$. Flowing Ar of 300 sccm was used to transport the $GaCl_3$ and $AlCl_3$ vapors to the deposition zone. Meanwhile, flowing NH_3 of 20 sccm was conveyed to the deposition zone by an inner quartz tube and reacted with the mixture of $GaCl_3$ and $AlCl_3$ vapors there for 4 h to produce the AlGaN nanocone arrays on the Si substrate. The system was then cooled to ambient temperature under the protection of Ar. To get a single phase $Al_xGa_{1-x}N$ nanocone, the matchable evaporation temperatures were optimized to be 70−90 °C for $GaCl_3$ and 130−150 °C for $AlCl_3$. By adjusting the evaporation temperatures of $GaCl_3$ and $AlCl_3$ precursors, the partial pressures of $GaCl_3$ and $AlCl_3$ vapors could be modulated, and the $Al_xGa_{1-x}N$ nanocones across the entire composition range were synthesized (Supporting Information, Figure S3).

The products were examined by SEM (Hitachi S-4800) equipped with an EDS detector. The microstructures of the products were characterized by XRD (Philips X'pert Pro X-ray diffractometer) with Cu Kα radiation of 0.15406 nm, HRTEM (JEM-2010, 200 kV) equipped with EDS, and SAED. Room-temperature CL experiments were carried out using a Gatan Mono CL3 spectrometer with an acceleration voltage of 10 kV. FE measurements were performed by using a parallel-plate configuration in a vacuum chamber at a pressure of ~7×10^{-5} Pa with a cathode−anode spacing of 100 μm.

Acknowledgment. This work was jointly supported by the "973" program (2007CB935503), NSFC (20873057, 20833002, 21073085), and the program for Changjiang Scholars and Innovative Research Team in University (PCSIRT). The authors thank Prof. Shuyuan Zhang of University of Science and Technology of China for technical help with HRTEM studies.

Supporting Information Available: (1) SEM images of the $Al_xGa_{1-x}N$ alloy nanocones with different compositions; (2) XRD analysis of the $Al_xGa_{1-x}N$ alloy nanocones; (3) XRD patterns and SEM images of phase-separated AlGaN nanocones; (4) HRTEM and SAED of the $Al_xGa_{1-x}N$ alloy nanocones; (5) TEM-EDS spectra for multiple-spot analysis along individual $Al_xGa_{1-x}N$ alloy nanocone; (6) field emission properties of the $Al_xGa_{1-x}N$ alloy nanocones. This material is available free of charge *via* the Internet at http://pubs.acs.org.

REFERENCES AND NOTES

1. Ponce, F. A.; Bour, D. P. Nitride-Based Semiconductors for Blue and Green Light-Emitting Devices. *Nature* **1997,** *386*, 351–359.
2. Mohammad, S. N.; Morkoc, H. Progress and Prospects of Group-III Nitride Semiconductors. *Prog. Quantum Electron.* **1996,** *20*, 361–525.
3. Ambacher, O. Growth and Applications of Group III-Nitrides. *J. Phys. D: Appl. Phys.* **1998,** *31*, 2653–2710.
4. Kung, P.; Razeghi, M. III-Nitride Wide Bandgap Semiconductors: A Survey of the Current Status and Future Trends of the Material and Device Technology. *Opto-Electron. Rev.* **2000,** *8*, 201–239.
5. Khan, A.; Balakrishnan, K.; Katona, T. Ultraviolet Light-Emitting Diodes Based on Group Three Nitrides. *Nat. Photonics* **2008,** *2*, 77–84.
6. Yoshida, H.; Yamashita, Y.; Kuwabara, M.; Kan, H. A 342-nm Ultraviolet AlGaN Multiple-Quantum-Well Laser Diode. *Nat. Photonics* **2008,** *2*, 551–554.
7. Yan, R. X.; Gargas, D.; Yang, P. D. Nanowire Photonics. *Nat. Photonics* **2009,** *3*, 569–576.
8. Huang, Y.; Duan, X. F.; Cui, Y.; Lieber, C. M. Gallium Nitride Nanowire Nanodevices. *Nano Lett.* **2002,** *2*, 101–104.
9. Huang, C. T.; Song, J. H.; Lee, W. F.; Ding, Y.; Gao, Z. Y.; Hao, Y.; Chen, L. J.; Wang, Z. L. GaN Nanowire Arrays for High-Output Nanogenerators. *J. Am. Chem. Soc.* **2010,** *132*, 4766–4771.
10. Lim, S. K.; Brewster, M.; Qian, F.; Li, Y.; Lieber, C. M.; Gradecak, S. Direct Correlation between Structural and Optical Properties of III−V Nitride Nanowire Heterostructures with Nanoscale Resolution. *Nano Lett.* **2009,** *9*, 3940–3944.
11. Chattopadhyay, S.; Ganguly, A.; Chen, K. H.; Chen, L. C. One-Dimensional Group III-Nitrides: Growth, Properties,

and Applications in Nanosensing and Nano-Optoelectronics. *Crit. Rev. Solid State Mater. Sci.* **2009**, *34*, 224–279.

12. Wu, Q.; Hu, Z.; Wang, X. Z.; Lu, Y. N.; Chen, X.; Xu, H.; Chen, Y. Synthesis and Characterization of Faceted Hexagonal Aluminum Nitride Nanotubes. *J. Am. Chem. Soc.* **2003,** *125*, 10176–10177.
13. Liu, C.; Hu, Z.; Wu, Q.; Wang, X. Z.; Chen, Y.; Sang, H.; Zhu, J. M.; Deng, S. Z.; Xu, N. S. Vapor−Solid Growth and Characterization of Aluminum Nitride Nanocones. *J. Am. Chem. Soc.* **2005,** *127*, 1318–1322.
14. He, C. Y.; Wang, X. Z.; Wu, Q.; Hu, Z.; Ma, Y. W.; Fu, J. J.; Chen, Y. Phase-Equilibrium-Dominated Vapor−Liquid−Solid Growth Mechanism. *J. Am. Chem. Soc.* **2010,** *132*, 4843–4847.
15. Chen, C. C.; Yeh, C. C.; Chen, C. H.; Yu, M. Y.; Liu, H. L.; Wu, J. J.; Chen, K. H.; Chen, L. C.; Peng, J. Y.; Chen, Y. F. Catalytic Growth and Characterization of Gallium Nitride Nanowires. *J. Am. Chem. Soc.* **2001,** *123*, 2791–2798.
16. Goldberger, J.; He, R. R.; Zhang, Y. F.; Lee, S. W.; Yan, H. Q.; Choi, H. J.; Yang, P. D. Single-Crystal Gallium Nitride Nanotubes. *Nature* **2003,** *422*, 599–602.
17. Kuykendall, T.; Pauzauskie, P. J.; Zhang, Y. F.; Goldberger, J.; Sirbuly, D.; Denlinger, J.; Yang, P. D. Crystallographic Alignment of High-Density Gallium Nitride Nanowire Arrays. *Nat. Mater.* **2004,** *3*, 524–528.
18. Vaddiraju, S.; Mohite, A.; Chin, A.; Meyyappan, M.; Sumanasekera, G.; Alphenaar, B. W.; Sunkara, M. K. Mechanisms of 1D Crystal Growth in Reactive Vapor Transport: Indium Nitride Nanowires. *Nano Lett.* **2005,** *5*, 1625–1631.
19. Kuykendall, T.; Ulrich, P.; Aloni, S.; Yang, P. D. Complete Composition Tunability of InGaN Nanowires Using a Combinatorial Approach. *Nat. Mater.* **2007,** *6*, 951–956.
20. Ristic, J.; Sanchez-Garcia, M. A.; Calleja, E.; Sanchez-Paramo, J.; Calleja, J. M.; Jahn, U.; Ploog, K. H. AlGaN Nanocolumns Grown by Molecular Beam Epitaxy: Optical and Structural Characterization. *Phys. Status Solidi A* **2002,** *192*, 60–66.
21. Choi, H. J.; Johnson, J. C.; He, R. R.; Lee, S. K.; Kim, F.; Pauzauskie, P.; Goldberger, J.; Saykally, R. J.; Yang, P. D. Self-Organized GaN Quantum Wire UV Lasers. *J. Phys. Chem. B* **2003,** *107*, 8721–8725.
22. Su, J.; Gherasimova, M.; Cui, G.; Tsukamoto, H.; Han, J.; Onuma, T.; Kurimoto, M.; Chichibu, S. F.; Broadbridge, C.; He, Y.; Nurmikko, A. V. Growth of AlGaN Nanowires by Metalorganic Chemical Vapor Deposition. *Appl. Phys. Lett.* **2005,** *87*, 183108.
23. Gaevski, M. E.; Sun, W.; Yang, J.; Adivarahan, V.; Sattu, A.; Mokina, I.; Shatalov, M.; Simin, G.; Khan, M. A. Non-Catalyst Growth and Characterization of *a*-Plane AlGaN Nanorods. *Phys. Status Solidi A* **2006,** *203*, 1696–1699.
24. Hong, L.; Liu, Z.; Zhang, X. T.; Hark, S. K. Self-Catalytic Growth of Single-Phase AlGaN Alloy Nanowires by Chemical Vapor Deposition. *Appl. Phys. Lett.* **2006,** *89*, 193105.
25. Park, Y. S.; Hwang, B. R.; Lee, J. C.; Im, H.; Cho, H. Y.; Kang, T. W.; Na, J. H.; Park, C. M. Self-Assembled $Al_xGa_{1-x}N$ Nanorods Grown on Si(001) Substrates by Using Plasma-Assisted Molecular Beam Epitaxy. *Nanotechnology* **2006,** *17*, 4640–4643.
26. Wang, X. B.; Song, J. H.; Zhang, F; He, C. Y.; Hu, Z.; Wang, Z. L. Electricity Generation Based on One-Dimensional Group-III Nitride Nanomaterials. *Adv. Mater.* **2010,** *22*, 2155–2158.
27. Li, Y.; Xiang, J.; Qian, F.; Gradecak, S.; Wu, Y.; Yan, H.; Blom, D. A.; Lieber, C. M. Dopant-Free GaN/AlN/AlGaN Radial Nanowire Heterostructures as High Electron Mobility Transistors. *Nano Lett.* **2006,** *6*, 1468–1473.
28. Nikishin, S. A.; Faleev, N. N.; Zubrilov, A. S.; Antipov, V. G.; Temkin, H. Growth of AlGaN on Si(111) by Gas Source Molecular Beam Epitaxy. *Appl. Phys. Lett.* **2000,** *76*, 3028–3030.
29. Iwaya, M.; Terao, S.; Sano, T.; Ukai, T.; Nakamura, R.; Kamiyama, S.; Amano, H.; Akasaki, I. Suppression of Phase Separation of AlGaN during Lateral Growth and Fabrication of High-Efficiency UV-LED on Optimized AlGaN. *J. Cryst. Growth* **2002,** *237*, 951–955.
30. Mattila, T.; Zunger, A. Predicted Bond Length Variation in Wurtzite and Zinc-Blende InGaN and AlGaN Alloys. *J. Appl. Phys.* **1999,** *85*, 160–167.
31. Vegard, L. The Constitution of the Mixed Crystals and the Filling of Space of the Atoms. *Z. Phys.* **1921,** *5*, 17–26.
32. Vayssieres, L.; Keis, K.; Hagfeldt, A.; Lindquist, S. Three-Dimensional Array of Highly Oriented Crystalline ZnO Microtubes. *Chem. Mater.* **2001,** *13*, 4395–4398.
33. Garcia, S. P.; Semancik, S. Controlling the Morphology of Zinc Oxide Nanorods Crystallized from Aqueous Solutions: The Effect of Crystal Growth Modifiers on Aspect Ratio. *Chem. Mater.* **2007,** *19*, 4016–4022.
34. Yao, K. X.; Zeng, H. C. Asymmetric ZnO Nanostructures with an Interior Cavity. *J. Phys. Chem. B* **2006,** *110*, 14736–14743.
35. Li, W. J.; Shi, E. W.; Zhong, W. Z.; Yin, Z. W. Growth Mechanism and Growth Habit of Oxide Crystals. *J. Cryst. Growth* **1999,** *203*, 186–196.
36. Hersee, S. D.; Sun, X. Y.; Wang, X. The Controlled Growth of GaN Nanowires. *Nano Lett.* **2006,** *6*, 1808–1811.
37. Yoshida, S.; Misawa, S.; Gonda, S. Properties of $Al_xGa_{1-x}N$ Films Prepared by Reactive Molecular Beam Epitaxy. *J. Appl. Phys.* **1982,** *53*, 6844–6848.
38. Yoshida, A. Bandedge and Optical Functions of AlN. In *Properties, Processing and Applications of Gallium Nitride and Related Semiconductors*; Edgar, J. H., Strite, S., Akasaki, I., Amano, H., Wetzel, C., Eds.; INSPEC: London, 1999; pp 31−39.
39. Choi, T. S.; Chung, M. S. Analysis of the Carrier Concentration for Field Emission from $Al_xGa_{1-x}N$. *Appl. Surf. Sci.* **2005,** *251*, 191–195.
40. She, J. C.; Xiao, Z. M.; Yang, Y. H.; Deng, S. Z.; Chen, J.; Yang, G. W.; Xu, N. S. Correlation between Resistance and Field Emission Performance of Individual ZnO One-Dimensional Nanostructures. *ACS Nano* **2008,** *2*, 2015–2022.